IEEE Access
Multidisciplinary ⋮ Rapid Review ⋮ Open Access Journal

Received February 14, 2020, accepted March 16, 2020, date of publication March 18, 2020, date of current version March 30, 2020.

Digital Object Identifier 10.1109/ACCESS.2020.2981717

Efficient Joint Channel Equalization and Tracking for V2X Communications Using SC-FDE Schemes

PEDRO PEDROSA[1], (Member, IEEE), DANIEL CASTANHEIRA[1], ADÃO SILVA[1,3], RUI DINIS[2,4], (Senior Member, IEEE), AND ATÍLIO GAMEIRO[1,3]
[1]Instituto de Telecomunicações, 3810-193 Aveiro, Portugal
[2]Instituto de Telecomunicações, 1049-001 Lisbon, Portugal
[3]DETI, Universidade de Aveiro, 3810-193 Aveiro, Portugal
[4]FCT, DEE, Universidade Nova de Lisboa, 2829-516 Caparica, Portugal

Corresponding author: Pedro Pedrosa (pmfopedrosa@av.it.pt)

This work was supported by the European Regional Development Fund (FEDER), through the Competitiveness and Internationalization Operational Program (COMPETE 2020) of the Portugal 2020 framework, Regional OP Centro (POCI-01-0145-FEDER-030588), Regional OP Lisboa (Lisboa-01-0145-FEDER-03058) and by FCT/MEC through national funds, under Project MASSIVE5G (PTDC/EEI-TEL/30588/2017), and PES3N (POCI-01-0145-FEDER-030629).

ABSTRACT Our aim with this paper is to present a solution suitable for vehicle-to-everything (V2X) communications, particularly, when employing single-carrier modulations combined with frequency-domain equalization (SC-FDE). In fact, we consider the V2X channel to be doubly-selective, where the variation of the channel in time is due to the presence of a Doppler term. Accordingly, the equalization procedure is dealt by a low-complexity iterative frequency-domain equalizer based on the iterative block decision-feedback equalization (IB-DFE) while the tracking procedure is conducted employing an extended Kalman filter (EKF). The proposed system is very efficient since it allows a very low density of training symbols, even for fast-varying channels. Furthermore only two training symbols are required to initialize the tracking procedure. Thus, ensuring low latency together with reduced channel estimation overheads.

INDEX TERMS Adaptive equalizers, channel estimation, digital communication, Kalman filters, signal processing, signal processing algorithms, vehicular and wireless technologies.

I. INTRODUCTION

Vehicles in intelligent transportation systems (ITS) are expected to be equipped with high-end video cameras as well as advanced environmental sensors [1], [2]. They will also depend on advanced mobile networks to achieve ubiquitous and prompt vehicle-to-everything (V2X) communications [3]–[7]. Exchanged data may include sensed data or maneuver plans with 3D scenes and interactions and reach payloads in the Gbps magnitude.

To support such expressive payloads, multi-standard solutions that combine both the dedicated short range communications (DSRC) channel of 802.11p with the millimeter wave (mmWave) communications of fifth generation new radio (5G NR) have been proposed [8], [9]. In fact, service requirements to support the next generation of V2X applications has been released by 3GPP. More specifically, in Release 16 with the normative works of 5G V2X services, and ultra-reliable low-latency communications (URLLC) [10]–[12], and in Release 17 with the enhancements to the application layer to support V2X services [13].

The vehicular channel is characterized by shadowing by third-party vehicles and high Doppler shifts due to the inherent non-stationary nature of the user terminals [14]. This is particularly significant in systems operating in the mmWave spectrum [15], [16], since Doppler effects are proportional to the carrier frequency.

In this work we address the inter-symbolic interference (ISI) stemming from multi-path propagation and the time-varying nature of the channel due to Doppler shifts. Accordingly, to cope with the strong ISI levels we propose single-carrier modulations combined with frequency-domain equalization (SC-FDE) [17]–[19]. Particularly, we will be using the iterative block-decision feedback equalizer (IB-DFE) [20], which can be regarded as a turbo equalizer implemented in the frequency domain [21]. As for the time-varying nature of the channel we consider the use of an extended Kalman filter (EKF) combined with an efficient

The associate editor coordinating the review of this manuscript and approving it for publication was Ki-Hong Park.

frame structure. With this approach we are able to track the channel variations while limiting the number of training blocks transmitted. In fact, by employing the EKF we are able to update the EKF during the transmission of the training blocks while predicting the channel during the transmission of the data blocks. Moreover, if a decision-directed approach is employed, updating the EKF is also possible during the transmission of the data blocks. Notably, the channel estimates produced by the EKF are employed in the equalization step to produce decisions on the transmitted symbols, decisions which in turn are used in the EKF to produce new channel estimates, recursively.

Notice that the Kalman filter is a well known solution to the problem of channel tracking [22]–[27]. In [22], Iltis addresses the problem of delay estimation in the presence of multipath using the EKF. In [23], Haykin *et al.* exploit the one-to-one correspondences between the recursive least-squares (RLS) and Kalman variables to formulate extended forms of the RLS algorithm. In [24], Komniakis *et al.* address the problem of channel tracking and equalization for multi-input multi-output (MIMO) channels. In [25], Simon *et al.* proposes a state-space approach that jointly estimates the multipath Rayleigh channel gains and the carrier frequency offset (CFO), and in [26] they propose a soft-Kalman filter. Similar approaches based on iterative detection and decoding are proposed in [27]–[29]. These use, nevertheless, channel coding which prevents a direct comparison with our solution.

A central element that distinguishes this work from the previous ones is the state-transition model. In fact, we see that in [22]–[27] the multipath complex channel gains are approximated by the basis expansion model (BEM) with an auto-regressive (AR) process used to characterize the variations of the weighting coefficients of the BEM across the frame. Differently, we assume that amplitude of the complex channel gains is static and that only the phase is variable. In fact, for broadband radio channels, where the number of contributions for each ray is small, and all contributions arrive more or less from the same direction, it is reasonable to admit that the amplitude varies at a much lower rate than the phase. Therefore, we consider the state-space vector to be formed by the phases of the complex gains and their associated Doppler terms. These assumptions results in a very simple state-transition model that has a clear and evident relation with the physics of the problem.

Relatively to our previous work [30], we have obtained the Bayesian Cramér-Rao bound (BCRB) for the the estimates of the state-vector elements. Namely, the complex channel gains and the Doppler terms. This a very important element in our investigation since through the knowledge of the BCRB it is possible to assess the performance of the proposed algorithm regarding its theoretical limits. Additionally, we have also investigated the convergence rate of the proposed algorithms. This was made through simulations which considered different distributions of the training symbols and lengths of the initial training stage. In this way different design choices are evaluated. In fact, these simulations provided valuable

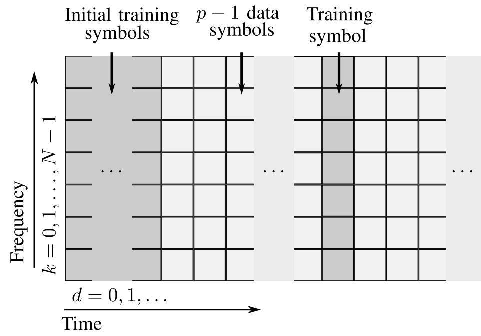

FIGURE 1. Frame structure.

insights on the behaviour of the proposed channel estimation algorithms. Finally, we have included more simulation scenarios so that it is now clear to see whether the proposed receiver still works well under demanding regimes. Particularly, when considering large values for the Doppler terms.

This work is organized as follows. In Sec. II we present the system model. Particularly, the channel model, channel equalization, and channel estimation. In Sec. III we formulate the channel tracking problem as a state-estimation problem and derive the EKF. In Sec. IV we discuss the performance results of the proposed system. Finally, in Sec. V we draw the conclusions for this work.

The notation used in this work is the following. Column vectors are denoted by small-case bold types (*e.g.*, $\boldsymbol{a}$); matrices are denoted by upper-case types (*e.g.*, $\boldsymbol{A}$); the identity matrix is $\boldsymbol{I}$ while the all-zeros matrix is $\mathbf{0}$. Depending on the context, $\mathbf{0}$ can also denote a column vector. Transpose, and conjugate, are denoted by $(\cdot)^\top$, and $(\cdot)^*$, respectively. Operations performed over vectors by scalar functions are assumed to happen element-wise (*e.g.*, if $\boldsymbol{v} = [v_1\, v_2]^\top$ then $\sin(\boldsymbol{v}) = [\sin(v_1)\ \sin(v_2)]^\top$). Operator $\mathrm{Var}(\cdot)$ returns the variance of its argument. $\mathrm{DFT}\{\cdot\}$, and $\mathrm{IDFT}\{\cdot\}$ denotes the discrete Fourier transform and its inverse, respectively. Operator $\mathrm{sign}(\cdot)$ is defined as

$$\mathrm{sign}(a) = \begin{cases} 1, & a \geq 0 \\ -1, & a < 0 \end{cases}$$

with $a \in \mathbb{R}$. Operators $\mathcal{R}(\cdot)$, and $\mathcal{I}(\cdot)$ are, respectively, the real and imaginary parts of a given complex number. $\mathrm{HD}\{\cdot\}$ denotes hard-decisions and is defined as $\mathrm{HD}\{\cdot\} \equiv \mathrm{sign}[\mathcal{R}(\cdot)] + j\mathrm{sign}[\mathcal{I}(\cdot)]$ with $j = \sqrt{-1}$. Finally, in Algorithm 1, and Algorithm 2 operators $a == b$, and $a \neq\neq b$ test integers a and b for equality, and inequality, respectively; $\mathrm{mod}(\cdot, \cdot)$ is the modulo operation.

II. SYSTEM MODEL

Consider the frame structure depicted in Fig. 1, where we have, at the beginning of the frame, M consecutive training symbols placed there for synchronization purposes. These training symbols are followed by data symbols interspersed with further training symbols. The training symbols are separated by $p-1$ data symbols. Each data symbol corresponds to an DFT-block with N subcarriers and has duration T_{B}. The duration of a training symbol is T_{TS} and can be equal or smaller than T_{B}. Both the training and the data symbols are preceded by a cyclic prefix whose duration T_{CP} is longer than the duration of the overall channel impulse response.

The transmitted signal associated to the frame is

$$s(t) = \sum_{d} s_d(t - dT_{\mathrm{B}}) \tag{1}$$

while the dth transmitted symbol has the form

$$s_d(t) = \sum_{n=-N_{\mathrm{G}}}^{N-1} s_{n,d}\, g(t - nT_{\mathrm{s}}) \tag{2}$$

with T_{s} denoting the symbol duration, N_G denoting the number of samples at the cyclic prefix and $g(t)$ the adopted pulse shaping filter. Clearly, $T_{\mathrm{s}} = T_{\mathrm{B}}/N$ and $N_G = T_{\mathrm{CP}}/T_{\mathrm{s}}$.

A. CHANNEL MODEL

We consider a broadband multipath radio channel, where the number of contributions for each ray are small and where all contributions arrive more or less from the same direction. In fact, if the number of contributions is small and if they all arrive more or less from the same direction then it is reasonable to admit that the amplitude varies at a much smaller rate than the phase.

Consider a multipath channel with L rays where each ray can be modeled by a complex exponential $\alpha_{l,d} \in \mathbb{C}$, $l = 1, \ldots, L$, and a delay relative to the principal ray τ_l, define $\varphi_{l,d} \triangleq \arg\{\alpha_{l,d}\}$, particularly $\varphi_{l,0} \triangleq \arg\{\alpha_{l,0}\}$, and assume the presence of a Doppler frequency shift term $\nu_l = f_D T_B \cos(\theta_l)$, where f_D, T_B, and θ_l are, respectively, the Doppler frequency, the symbol duration, and the angle of arrival, then $\varphi_{l,d} = \varphi_{l,0} + 2\pi d \nu_l$ and the model for the continuous channel impulse response (CIR) is

$$\begin{aligned} h(t, dT_B) &= \sum_{l=1}^{L} \alpha_{l,0} \exp(j2\pi d\nu_l)\delta(t - \tau_l) \\ &= \sum_{l=1}^{L} |\alpha_{l,0}| \exp(j\varphi_{l,d})\delta(t - \tau_l) \\ &= \sum_{l=1}^{L} \alpha_{l,d}\delta(t - \tau_l). \end{aligned} \tag{3}$$

The continuous channel frequency response (CFR) $H_d(f)$, is given by

$$H_d(f) = \sum_{l=1}^{L} \alpha_{l,d} \exp(-j2\pi f \tau_l), \tag{4}$$

while the discrete version is $H_{k,d} = H_d(f)|_{f=\frac{k}{T_{\mathrm{B}}}}$, with $k = 0, 1, \ldots, N-1$.

Further considering that $\{h_{n,d};\, n = 0, 1, \ldots, N-1\} = \mathrm{IDFT}\{H_{k,d};\, k = 0, 1, \ldots, N-1\}$ and assuming that

- the sampling occurs at instants $\{\tau_l;\, l = 0, 1, \ldots, L-1\}$,

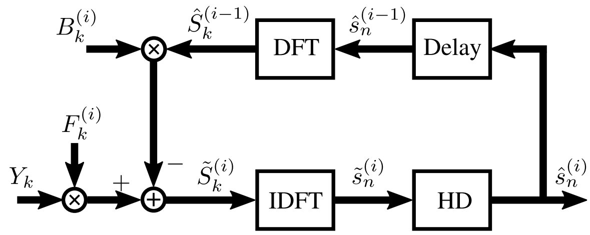

FIGURE 2. A general overview of the IB-DFE scheme.

- we have $L = N_{\mathrm{CP}}$ rays, with most of rays equal to zero,

then we have that $\{\alpha_{l,d};\, l = 0, 1, \ldots, L-1\} = \{h_{n,d};\, n = 0, 1, \ldots, N_{\mathrm{CP}}-1\}$. Finally, and since we are assuming that the complex channel gains $\alpha_{l,d}$ have constant amplitude in time (i.e., regarding d), particularly, $|\alpha_{l,d}| = |\alpha_{l,0}|$, then to observe the channel variation is equivalent to obtain $\alpha_{l,d}/|\alpha_{l,d}|$.

B. CHANNEL EQUALIZATION

Unlike OFDM, with SC-FDE the cyclic prefix (CP) does not solve the problem of ISI. In fact, if we distinguish the interference between transmitted symbols from the interference between DFT-blocks, the CP solves the latter but we still have the former with SC-FDE. Accordingly, provided that the received signal has a CP longer than the overall channel impulse response the frequency-domain received signal is given by

$$Y_{k,d} = S_{k,d}H_{k,d} + N_{k,d}, \quad \begin{aligned} &k = 0, 1, \ldots, N-1, \\ &d = 0, 1, \ldots \end{aligned} \tag{5}$$

where the frequency-domain samples $\{S_{k,d};\, k = 0, 1, \ldots, N-1\}$ are the discrete Fourier transform (DFT) of the time-domain transmitted symbols $\{s_{n,d};\, n = 0, 1, \ldots, N-1\}$, i.e., $\{S_{k,d};\, k = 0, 1, \ldots, N-1\} = \mathrm{DFT}\{s_{n,d};\, n = 0, 1, \ldots, N-1\}$, and $\{N_{k,d};\, k = 0, 1, \ldots, N-1\}$ is the channel noise in the frequency-domain. We also assume that the channel fading during one DFT-block is almost constant. In fact, if one knows the phase noise and/or the carrier frequency offset (CFO) then the phase variations occurring inside the block be compensated [31], thus ensuring the time-invariant property of the block.

Clearly, the impact of the time dispersive channel reduces to a scaling factor for each subcarrier. To cope with the residual effects of the channel we can employ a linear FDE. However, the performance is much better if the linear FDE is replaced by an IB-DFE [20]. The block diagram of an IB-DFE scheme is depicted in Fig. 2.

Consider that for the ith iteration the frequency-domain samples at the output of the IB-DFE are given by

$$\tilde{S}_{k,d}^{(i)} = F_{k,d}^{(i)} Y_{k,d} - B_{k,d}^{(i)} \hat{S}_{k,d}^{(i-1)}, \quad \begin{aligned} &k = 0, 1, \ldots, N-1, \\ &d = 0, 1, \ldots \end{aligned} \tag{6}$$

where $\{F_{k,d}^{(i)};\, k = 0, 1, \ldots, N-1\}$ are the feedforward coefficients, and $\{B_{k,d}^{(i)};\, k = 0, 1, \ldots, N-1\}$ are the feedback coefficients. $\{\hat{S}_{k,d}^{(i-1)};\, k = 0, 1, \ldots, N-1\}$ denotes the DFT of the time-domain decisions obtained in the previous iteration, *i.e*, $\{\hat{S}_{k,d}^{(i-1)}; k = 0,1,\ldots,N-1\} = \mathrm{DFT}\{\hat{s}_{n,d}^{(i-1)}; n = 0,1,\ldots,N-1\}$ with $\{\hat{s}_{n,d}^{(i-1)}; n = 0,1,\ldots,N-1\} = \mathrm{HD}\{\tilde{s}_{n,d}^{(i-1)}; n = 0,1,\ldots,N-1\}$, where $\{\tilde{s}_{n,d}^{(i)}; n = 0,1,\ldots,N-1\} = \mathrm{IDFT}\{\tilde{S}_{k,d}^{(i)}; k = 0,1,\ldots,N-1\}$.

The derivation of the filtering coefficients can be found in the literature (see, e.g., [32]) and their optimal values are reproduced here for convenience only. Therefore, for QPSK constellations the expressions for the feedback, and feedforward coefficients are respectively,

$$B_{k,d}^{(i)} = F_{k,d}^{(i)} H_{k,d} - 1, \quad \begin{array}{l} k = 0,1,\ldots,N-1, \\ d = 0,1,\ldots \end{array} \tag{7}$$

and

$$F_{k,d}^{(i)} = \frac{\breve{F}_{k,d}^{(i)}}{\gamma_d^{(i)}}, \quad \begin{array}{l} k = 0,1,\ldots,N-1, \\ d = 0,1,\ldots \end{array} \tag{8}$$

where

$$\breve{F}_{k,d}^{(i)} = \frac{H_{k,d}^*}{\alpha_d + (1-(\rho_d^{(i-1)})^2)|H_{k,d}|^2}, \quad \begin{array}{l} k = 0,1,\ldots,N-1, \\ d = 0,1,\ldots \end{array} \tag{9}$$

and the reciprocal of the signal-to-noise ratio (SNR) $\alpha_d = E[|N_{k,d}|^2]/E[|S_{k,d}|^2]$,

$$\gamma_d^{(i)} = \frac{1}{N}\sum_{k=0}^{N-1} \breve{F}_{k,d}^{(i)} H_{k,d}, \quad d = 0,1,\ldots \tag{10}$$

The feedback reliability $\rho_d^{(i-1)}$ is given by,

$$\rho_d^{(i-1)} = \frac{E[\hat{s}_{n,d}^{(i-1)} s_{n,d}^*]}{E[|s_{n,d}|^2]}, \quad d = 0,1,\ldots \tag{11}$$

Notice that we consider the SNR to be known. Notably, SNR estimation techniques like the ones proposed in [33], and [34], where the SNR is inferred from the feedback reliability (11), can be easily implemented at the receiver.

C. CHANNEL ESTIMATION

Equalizer coefficients (7), and (8), are functions of the CFR. Thus it is fundamental to provide the equalizer with good estimates of the channel. Noticing that the received signal is (5) a least-squares (LS), an estimate of the CFR is readily available by doing

$$\tilde{H}_{k,d} = \frac{Y_{k,d}}{S_{k,d}}, \quad \begin{array}{l} k = 0,1,\ldots,N-1, \\ d = 0,1,\ldots \end{array} \tag{12}$$

Naturally, $\{S_{k,d}; k = 0,1,\ldots,N-1\}$ is not available at the receiver unless it is a known training sequence $\{S_k^{\mathrm{TS}}; k = 0,1,\ldots,N-1\}$. Alternatively, one can use the decisions on the transmitted symbols $\{\hat{S}_{k,d}; k = 0,1,\ldots,N-1\}$. We will designate the former approach training symbol (TS) channel estimation and the latter decision-directed (DD) channel estimation.

Alternatively, instead of (12) one can obtain a minimum mean-squared error (MMSE) estimate [35]

$$\tilde{H}_{k,d} = \frac{Y_{k,d} S_{k,d}^*}{|S_{k,d}|^2 + SNR^{-1}}, \quad \begin{array}{l} k = 0,1,\ldots,N-1, \\ d = 0,1,\ldots \end{array} \tag{13}$$

where $SNR^{-1} = \mathrm{E}[|N_k|^2]/\mathrm{E}[|S_k|^2]$ is the reciprocal of the signal-to-noise ratio (SNR).

Notice that in (13), one can choose training symbols with constant amplitude whereby the use of the MMSE makes no sense. However, if we employ decision symbols then the use of the MMSE is justified, since $\{|S_{k,d}|; k = 0,1,\ldots,N-1\}$ is approximately Gaussian.

III. CHANNEL TRACKING

In this section we present an EKF specially designed for tracking a time-varying channel where the time-variation is due to the presence of a Doppler term.

A. THE EKF FOR CHANNEL TRACKING

1) PROCESS MODEL

The process (or state-transition) model captures the rules governing the state dynamics. Assuming that the state vector is $\boldsymbol{x}_d = [\boldsymbol{\nu}^\top \ \boldsymbol{\varphi}_d^\top]^\top$, where $\boldsymbol{\nu} = [\nu_1 \ldots \nu_L]^\top$, and $\boldsymbol{\varphi}_d = [\varphi_{1,d} \ldots \varphi_{L,d}]^\top$ then the state-transition equation is

$$\boldsymbol{x}_{d+p} = \boldsymbol{H}^{(p)} \boldsymbol{x}_d, \tag{14}$$

where $\boldsymbol{H}^{(p)}$ is the p-step state-transition matrix

$$\boldsymbol{H}^{(p)} = \begin{bmatrix} \boldsymbol{I}_L & \boldsymbol{0}_L \\ 2\pi p \boldsymbol{I}_L & \boldsymbol{I}_L \end{bmatrix}. \tag{15}$$

2) OBSERVATION MODEL

Defining the non-linear vector function,

$$\boldsymbol{f}(\boldsymbol{\varphi}_d) = \left[[f_1(\boldsymbol{\varphi}_d)]^\top \ [f_2(\boldsymbol{\varphi}_d)]^\top \right]^\top, \tag{16}$$

with $f_1(\boldsymbol{\varphi}_d) = \cos(\boldsymbol{\varphi}_d)$, and $f_2(\boldsymbol{\varphi}_d) = \sin(\boldsymbol{\varphi}_d)$ results for the observation vector $\boldsymbol{z}_d = [z_{1,d} \ldots z_{L,d}]^\top$,

$$\boldsymbol{z}_d = \boldsymbol{f}(\boldsymbol{\varphi}_d) + \boldsymbol{v}_d, \tag{17}$$

where $\boldsymbol{v}_d = [v_{1,d} \ldots v_{L,d}]^\top$ is the observation noise vector.

The observation's noise covariance matrix is $\boldsymbol{R} = \sigma_v^2 \boldsymbol{I}$, where σ_v^2 is the variance of the real (imaginary) part of the complex white Gaussian noise process $\{v_{l,d}; l = 0,1,\ldots,L-1; d = 0,1,2,\ldots\}$. The elements of the noise vector $\boldsymbol{v}_d$ are independent and identically distributed.

Notice that the variance of the observation noise is different if we consider the channel estimates to result from training symbols or from the decision-directed approach. To distinguish both cases we use a superscript on the channel observation noise covariance matrix. Namely, $\boldsymbol{R}^{\mathrm{TS}}$ for the training symbol case and $\boldsymbol{R}^{\mathrm{DD}}$ for the decision-directed case.

3) PREDICTION STAGE (AT THE TRAINING SYMBOLS)

If the dth symbol is a training symbol, with $d = 0, p, 2p, \ldots$, then the prediction stage corresponds to the computation of the pth-order *a priori* state-mean $\boldsymbol{x}_{d|d-p}$, and state-covariance $\boldsymbol{P}_{d|d-p}$, using the pth-order *a posteriori* state-mean $\boldsymbol{x}_{d-p|d-p}$, and state-covariance $\boldsymbol{P}_{d-p|d-p}$, obtained during the previous training symbol. Accordingly,

$$\boldsymbol{x}_{d|d-p} = \boldsymbol{H}^{(p)}\boldsymbol{x}_{d-p|d-p}, \tag{18a}$$

$$\boldsymbol{P}_{d|d-p} = \boldsymbol{H}^{(p)}\boldsymbol{P}_{d-p|d-p}\boldsymbol{H}^{(p)\top}. \tag{18b}$$

4) UPDATE STAGE (AT THE TRAINING SYMBOLS)

The update stage, which without a decision-directed approach for the channel estimation occurs only at the training symbols, combines the *a priori* state-mean $\boldsymbol{x}_{d|d-p}$ with the so-called measurement residual $\boldsymbol{e}_d$, resulting in a refined state estimate. Accordingly, the *a posteriori* state-mean $\boldsymbol{x}_{d|d}$ and state-covariance matrix $\boldsymbol{P}_{d|d}$ are given by

$$\boldsymbol{x}_{d|d} = \boldsymbol{x}_{d|d-p} + \boldsymbol{K}_d\boldsymbol{e}_d, \tag{19a}$$

$$\boldsymbol{P}_{d|d} = (\boldsymbol{I} - \boldsymbol{K}_d\boldsymbol{J}_{d|d-p})\boldsymbol{P}_{d|d-p}, \tag{19b}$$

where $\boldsymbol{K}_d$ is the Kalman gain and $\boldsymbol{J}_{d|d-p}$ the Jacobian of (16) evaluated with respect to the prediction state-mean $\boldsymbol{x}_{d|d-p}$, *i.e.*,

$$\boldsymbol{J}_{d|d-p} = \boldsymbol{J}(\boldsymbol{x}_d)|_{\boldsymbol{x}_d=\boldsymbol{x}_{d|d-p}}. \tag{20}$$

For the derivation of the Jacobian see Sec. III-A7.

5) MEASUREMENT RESIDUAL

The measurement residual corresponds to,

$$\boldsymbol{e}_d = z_d^{\mathrm{TS}} - \boldsymbol{f}(\boldsymbol{\varphi}_{d|d-1}) = \begin{bmatrix} \mathcal{R}\{\hat{\boldsymbol{\alpha}}_d^{\mathrm{TS}}\}/|\hat{\boldsymbol{\alpha}}_d^{\mathrm{TS}}| \\ \mathcal{I}\{\hat{\boldsymbol{\alpha}}_d^{\mathrm{TS}}\}/|\hat{\boldsymbol{\alpha}}_d^{\mathrm{TS}}| \end{bmatrix} - \begin{bmatrix} \cos(\boldsymbol{\varphi}_{d|d-1}) \\ \sin(\boldsymbol{\varphi}_{d|d-1}) \end{bmatrix}. \tag{21}$$

where $\hat{\boldsymbol{\alpha}}_d^{\mathrm{TS}}$ is the vector of the channel estimates $\hat{\boldsymbol{\alpha}}_d^{\mathrm{TS}} = \left[\hat{\alpha}_{1,d}^{\mathrm{TS}} \ldots \hat{\alpha}_{L,d}^{\mathrm{TS}}\right]$ obtained through training symbols.

6) KALMAN GAIN

In (19a), $\boldsymbol{K}_d$ is the Kalman gain

$$\boldsymbol{K}_d = \boldsymbol{P}_{d|d-p}\boldsymbol{J}_{d|d-p}\boldsymbol{S}_d^{-1}, \tag{22}$$

where $\boldsymbol{S}_d$ is the residual covariance matrix,

$$\boldsymbol{S}_d = \boldsymbol{R}^{\mathrm{TS}} + \boldsymbol{J}_{d|d-p}\boldsymbol{P}_{d|d-p}\boldsymbol{J}_{d|d-p}^{\top}. \tag{23}$$

7) JACOBIAN DERIVATION

The EKF is derived by approximating the nonlinear observation function (16) by the first term in its Taylor series expansion evaluated at the estimated state vector. The first term of the Taylor series corresponds to the

TABLE 1. The EKF for channel tracking.

```
Require: R^TS
  for all d = 0, 1, ... do
    if mod(d, p) == 0 then {the dth symbol is a training symbol; d = 0, p, 2p, ...}
      if d == 0 then {Initialize the filter (see Sec. III-C1)}
        x_{0|0} ← x^init
        P_{0|0} ← P^init
      end if
      x_{d|d-p} ← H^(p) x_{d-p|d-p}
      P_{d|d-p} ← H^(p) P_{d-p|d-p} H^(p)⊤
      J_{d|d-p} ← J(x_d)|_{x_d = x_{d|d-p}}
      S_d ← R^TS + J_{d|d-p} P_{d|d-p} J^⊤_{d|d-p}
      K_d ← P_{d|d-p} J_{d|d-p} S_d^{-1}
      α̂_d^TS ← [α̂_{1,d}^TS ··· α̂_{L,d}^TS]^⊤
      e_d ← [R{α̂_d^TS}/|α̂_d^TS| ; I{α̂_d^TS}/|α̂_d^TS|] − [cos(φ_{d|d-p}) ; sin(φ_{d|d-p})]
      x_{d|d} ← x_{d|d-p} + K_d e_d
      P_{d|d} ← (I − K_d J_{d|d-p}) P_{d|d-p}
      x̂_d ← x_{d|d}
    else if mod(d, p) ≠≠ 0 then {the dth symbol is a data symbol; d = p + h; h = 1, 2, ..., p − 1}
      h ← mod(d, p)
      x_{d|d-h} ← H^(h) x_{d-h|d-h}
      x̂_d ← x_{d|d-h}
    end if
  end for
```

Jacobian

$$\boldsymbol{J}(\boldsymbol{x}_d) = \frac{\partial \boldsymbol{f}(\boldsymbol{\varphi}_d)}{\partial \boldsymbol{x}_d} = \begin{bmatrix} \frac{\partial f_1(\boldsymbol{\varphi}_d)}{\partial \boldsymbol{\nu}} & \frac{\partial f_1(\boldsymbol{\varphi}_d)}{\partial \boldsymbol{\varphi}_d} \\ \frac{\partial f_2(\boldsymbol{\varphi}_d)}{\partial \boldsymbol{\nu}} & \frac{\partial f_2(\boldsymbol{\varphi}_d)}{\partial \boldsymbol{\varphi}_d} \end{bmatrix} = \begin{bmatrix} \boldsymbol{0}_L & [f_1'(\boldsymbol{\varphi}_d)]^{\top}\boldsymbol{I}_L \\ \boldsymbol{0}_L & [f_2'(\boldsymbol{\varphi}_d)]^{\top}\boldsymbol{I}_L \end{bmatrix} \tag{24}$$

where $f_1'(\boldsymbol{\varphi}_d) = -\sin(\boldsymbol{\varphi}_d)$, and $f_2'(\boldsymbol{\varphi}_d) = \cos(\boldsymbol{\varphi}_d)$.

8) PREDICTION STAGE (AT THE DATA SYMBOLS)

If the dth symbol is a data symbol, with $d = p + h$, and $h = 1, 2, \ldots, p - 1$, then the *a posteriori* state-mean $\boldsymbol{x}_{d-h|d-h}$ can be used to obtain the state-mean prediction $\boldsymbol{x}_{d|d-h}$. Accordingly,

$$\boldsymbol{x}_{d|d-h} = \boldsymbol{H}^{(h)}\boldsymbol{x}_{d-h|d-h}, \tag{25}$$

where

$$\boldsymbol{H}^{(h)} = \begin{bmatrix} \boldsymbol{I}_L & \boldsymbol{0}_L \\ 2\pi h\boldsymbol{I}_L & \boldsymbol{I}_L \end{bmatrix}. \tag{26}$$

The state-estimate $\hat{\boldsymbol{x}}_d$, to be used in constructing an estimate of the CFR, is obtained from the state-mean prediction $\boldsymbol{x}_{d|d-h}$, *i.e.*, $\hat{\boldsymbol{x}}_d = \boldsymbol{x}_{d|d-h}$. Algorithm Table 1 lists the steps for the operation of the EKF for channel tracking.

Notice that since we are considering the use of training symbols only, we have no observations of the channel while transmitting the data symbols.Consequently, there is no update stage. In order to circumvent this limitation we propose a decision-directed approach to obtain state-observations during data transmission as well.

B. THE EKF WITH DECISION-DIRECTED CHANNEL ESTIMATION

When employing decision-directed channel estimates we are able to perform a prediction and update steps on both training and data symbols. Accordingly, the state-mean and state-covariance equations have unit-step prediction and update equations.

1) PREDICTION STAGE (AT THE TRAINING SYMBOLS)

The prediction state-mean and state-covariance are, respectively,

$$\boldsymbol{x}_{d|d-1} = \boldsymbol{H}\boldsymbol{x}_{d-1|d-1}, \tag{27a}$$

$$\boldsymbol{P}_{d|d-1} = \boldsymbol{H}\boldsymbol{P}_{d-1|d-1}\boldsymbol{H}^\top, \tag{27b}$$

where

$$\boldsymbol{H} = \begin{bmatrix} \boldsymbol{I}_L & 0_L \\ 2\pi\boldsymbol{I}_L & \boldsymbol{I}_L \end{bmatrix}. \tag{28}$$

2) UPDATE STAGE (AT THE TRAINING SYMBOLS)

The updated state-mean, and state-covariance, respectively,

$$\boldsymbol{x}_{d|d} = \boldsymbol{x}_{d|d-1} + \boldsymbol{K}_d\boldsymbol{e}_d, \tag{29a}$$

$$\boldsymbol{P}_{d|d} = (\boldsymbol{I} - \boldsymbol{K}_d\boldsymbol{J}_{d|d-1})\boldsymbol{P}_{d|d-1}, \tag{29b}$$

where the Jacobian is evaluated with respect to the posterior state-mean (27a), *i.e.*, $\boldsymbol{J}_{d|d-1} = \boldsymbol{J}(\boldsymbol{x}_d)|_{\boldsymbol{x}_d=\boldsymbol{x}_{d|d-1}}$.

The Kalman gain is

$$\boldsymbol{K}_d = \boldsymbol{P}_{d|d-1}\boldsymbol{J}_{d|d-1}\boldsymbol{S}_d^{-1}, \tag{30}$$

and the innovation covariance matrix

$$\boldsymbol{S}_d = \boldsymbol{R}^{\mathrm{TS}} + \boldsymbol{J}_{d|d-1}\boldsymbol{P}_{d|d-1}\boldsymbol{J}_{d|d-1}^\top. \tag{31}$$

3) PREDICTION AND UPDATE STAGES (AT THE DATA SYMBOLS)

The prediction and update stages of the EKF during the transmission of data symbols evaluates the same expressions as in the transmission of the training symbols, *i.e.*, (27a)–(29b). Except that the state-observations are now obtained using decision-directed channel estimation. Accordingly, the state-observation noise covariance matrix used to compute the innovations covariance matrix (31) is $\boldsymbol{R}^{\mathrm{DD}}$. Algorithm in Table 2 lists the steps for the operation of the EKF with DD channel observations.

Notice that, the state-estimate $\hat{\boldsymbol{x}}_d$ obtained at the pilot symbols results from the posterior state-mean, $\boldsymbol{x}_{d|d}$ while at the data symbols it results from the prediction state-mean $\boldsymbol{x}_{d|d-1}$. The state-estimate is used to produce an estimate $\hat{H}_d(f)$ of the CFR (4). In fact, using the state-estimate vector $\hat{\boldsymbol{x}}_d = [\hat{\boldsymbol{\nu}}_d^\top \ \hat{\boldsymbol{\varphi}}_d^\top]^\top$, particularly $\hat{\boldsymbol{\varphi}}_d = [\hat{\varphi}_{1,d} \ \ldots \ \hat{\varphi}_{L,d}]^\top$, we produce the estimate

$$\hat{H}_d(f) = \sum_{l=1}^{L} |\alpha_{l,0}| \exp\left[j(\hat{\varphi}_{l,d} - 2\pi f\tau_l)\right]. \tag{32}$$

TABLE 2. The EKF with DD channel observations.

Require: $\boldsymbol{R}^{\mathrm{TS}}, \boldsymbol{R}^{\mathrm{DD}}$
  for all $d = 0, 1, \ldots$ **do**
    if $\mathrm{mod}(d, p) == 0$ **then** {the dth symbol is a training symbol; $d = 0, p, 2p, \ldots$}
      if $d == 0$ **then** {Initialize the filter (see Sec. III-C1)}
        $\boldsymbol{x}_{0|0} \leftarrow \boldsymbol{x}^{\mathrm{init}}$
        $\boldsymbol{P}_{0|0} \leftarrow \boldsymbol{P}^{\mathrm{init}}$
      end if
      $\boldsymbol{x}_{d|d-1} \leftarrow \boldsymbol{H}\boldsymbol{x}_{d-1|d-1}$
      $\boldsymbol{P}_{d|d-1} \leftarrow \boldsymbol{H}\boldsymbol{P}_{d-1|d-1}\boldsymbol{H}^\top$
      $\boldsymbol{J}_{d|d-1} \leftarrow \boldsymbol{J}(\boldsymbol{x}_d)|_{\boldsymbol{x}_d=\boldsymbol{x}_{d|d-1}}$
      $\boldsymbol{S}_d \leftarrow \boldsymbol{R}^{\mathrm{TS}} + \boldsymbol{J}_{d|d-1}\boldsymbol{P}_{d|d-1}\boldsymbol{J}_{d|d-1}^\top$
      $\boldsymbol{K}_d \leftarrow \boldsymbol{P}_{d|d-1}\boldsymbol{J}_{d|d-1}\boldsymbol{S}_d^{-1}$
      $\hat{\boldsymbol{\alpha}}_d^{\mathrm{TS}} \leftarrow [\hat{\alpha}_{1,d}^{\mathrm{TS}} \cdots \hat{\alpha}_{L,d}^{\mathrm{TS}}]^\top$
      $\boldsymbol{e}_d \leftarrow \begin{bmatrix} \mathcal{R}\{\hat{\boldsymbol{\alpha}}_d^{\mathrm{TS}}\}/|\hat{\boldsymbol{\alpha}}_d^{\mathrm{TS}}| \\ \mathcal{I}\{\hat{\boldsymbol{\alpha}}_d^{\mathrm{TS}}\}/|\hat{\boldsymbol{\alpha}}_d^{\mathrm{TS}}| \end{bmatrix} - \begin{bmatrix} \cos(\boldsymbol{\varphi}_{d|d-1}) \\ \sin(\boldsymbol{\varphi}_{d|d-1}) \end{bmatrix}$
      $\boldsymbol{x}_{d|d} \leftarrow \boldsymbol{x}_{d|d-1} + \boldsymbol{K}_d\boldsymbol{e}_d$
      $\boldsymbol{P}_{d|d} \leftarrow (\boldsymbol{I} - \boldsymbol{K}_d\boldsymbol{J}_{d|d-1})\boldsymbol{P}_{d|d-1}$
      $\hat{\boldsymbol{x}}_d \leftarrow \boldsymbol{x}_{d|d}$
    else if $\mathrm{mod}(d, p) \neq\neq 0$ **then** {the dth symbol is a data symbol; $d = p + h; h = 1, 2, \ldots, p-1$}
      $\boldsymbol{x}_{d|d-1} \leftarrow \boldsymbol{H}\boldsymbol{x}_{d-1|d-1}$
      $\boldsymbol{P}_{d|d-1} \leftarrow \boldsymbol{H}\boldsymbol{P}_{d-1|d-1}\boldsymbol{H}^\top$
      $\hat{\boldsymbol{x}}_d \leftarrow \boldsymbol{x}_{d|d-1}$
      $\boldsymbol{J}_{d|d-1} \leftarrow \boldsymbol{J}(\boldsymbol{x}_d)|_{\boldsymbol{x}_d=\boldsymbol{x}_{d|d-1}}$
      $\boldsymbol{S}_d \leftarrow \boldsymbol{R}^{\mathrm{DD}} + \boldsymbol{J}_{d|d-1}\boldsymbol{P}_{d|d-1}\boldsymbol{J}_{d|d-1}^\top$
      $\boldsymbol{K}_d \leftarrow \boldsymbol{P}_{d|d-1}\boldsymbol{J}_{d|d-1}\boldsymbol{S}_d^{-1}$
      $\hat{\boldsymbol{\alpha}}_d^{\mathrm{DD}} \leftarrow [\hat{\alpha}_{1,d}^{\mathrm{DD}} \cdots \hat{\alpha}_{L,d}^{\mathrm{DD}}]^\top$
      $\boldsymbol{e}_d \leftarrow \begin{bmatrix} \mathcal{R}\{\hat{\boldsymbol{\alpha}}_d^{\mathrm{DD}}\}/|\hat{\boldsymbol{\alpha}}_d^{\mathrm{DD}}| \\ \mathcal{I}\{\hat{\boldsymbol{\alpha}}_d^{\mathrm{DD}}\}/|\hat{\boldsymbol{\alpha}}_d^{\mathrm{DD}}| \end{bmatrix} - \begin{bmatrix} \cos(\boldsymbol{\varphi}_{d|d-1}) \\ \sin(\boldsymbol{\varphi}_{d|d-1}) \end{bmatrix}$
      $\boldsymbol{x}_{d|d} \leftarrow \boldsymbol{x}_{d|d-1} + \boldsymbol{K}_d\boldsymbol{e}_d$
      $\boldsymbol{P}_{d|d} \leftarrow (\boldsymbol{I} - \boldsymbol{K}_d\boldsymbol{J}_{d|d-1})\boldsymbol{P}_{d|d-1}$
    end if
  end for

C. FILTER OPERATION

In this section we deal with issues related with the operation of the EKF. Namely, initialization and training stages.

1) INITIALIZATION

The EKF is initialized by assigning

$$\boldsymbol{x}_{0|0} = \boldsymbol{x}^{\mathrm{init}} \tag{33}$$

$$\boldsymbol{P}_{0|0} = \boldsymbol{P}^{\mathrm{init}} \tag{34}$$

and by using, at the prediction stage, the state-transition matrix

$$\boldsymbol{H}^{\mathrm{init}} = \begin{bmatrix} \boldsymbol{I}_L & 0_L \\ 2\pi\boldsymbol{I}_L & \boldsymbol{I}_L \end{bmatrix}. \tag{35}$$

2) TRAINING STAGE

In order to produce an initial estimate of the channel state variables, namely the Doppler rates and the path phases, we start the frame with a set of N_{train} training symbols. These symbols produce not only the initial estimate of the state-vector but ensure also a faster convergence of the EKF.

D. RECURSIVE BAYESIAN Cramér-RAO BOUND

In order to determine the best performance achievable by the EKF we resort to the results of [36], where Tichavský *et al.*

propose a recursive BCRB. Accordingly, the recursion for the Fisher information matrix [36] is

$$\boldsymbol{J}_{d+1} = \left(\boldsymbol{H}_d \boldsymbol{J}_d^{-1} \boldsymbol{H}_d^T\right)^{-1} + \mathrm{E}_{\boldsymbol{x}_{d+1}}\left\{\boldsymbol{D}_{d+1}^T \boldsymbol{R}_{d+1}^{-1} \boldsymbol{D}_{d+1}\right\}. \quad (36)$$

Defining,

$$\boldsymbol{J}_d = \begin{bmatrix} J_d^{\nu\nu} & J_d^{\nu\varphi} \\ J_d^{\nu\varphi} & J_d^{\varphi\varphi} \end{bmatrix}, \quad (37)$$

the first term on the right-hand-side of (36) is,

$$\left(\boldsymbol{H}_d \boldsymbol{J}_d^{-1} \boldsymbol{H}_d^T\right)^{-1} = \begin{bmatrix} (2\pi)^2 J_d^{\varphi\varphi} - 4\pi J_d^{\nu\varphi} + J_d^{\nu\nu} & -2\pi J_d^{\varphi\varphi} + J_d^{\nu\varphi} \\ -2\pi J_d^{\varphi\varphi} + J_d^{\nu\varphi} & J_d^{\varphi\varphi} \end{bmatrix} \quad (38)$$

Noting that matrix $\boldsymbol{D}_{d+1}$ is the Jacobian of the observation function (16) results for the 2nd term on the right-hand-side of (36),

$$\mathrm{E}_{\boldsymbol{x}_{d+1}}\left\{\boldsymbol{D}_{d+1}^T \boldsymbol{R}_{d+1}^{-1} \boldsymbol{D}_{d+1}\right\} = \frac{2}{\sigma_v^2}\begin{bmatrix} 0 & 0 \\ 0 & 1 \end{bmatrix}. \quad (39)$$

Adding the two terms, (38), and (39), results in the following recursive expression,

$$\boldsymbol{J}_{d+1} = \begin{bmatrix} (2\pi)^2 J_d^{\varphi\varphi} - 4\pi J_d^{\nu\varphi} + J_d^{\nu\nu} & -2\pi J_d^{\varphi\varphi} + J_d^{\nu\varphi} \\ -2\pi J_d^{\varphi\varphi} + J_d^{\nu\varphi} & J_d^{\varphi\varphi} + \dfrac{2}{\sigma_v^2} \end{bmatrix}. \quad (40)$$

Notice that, the elements of the Fisher information matrix is associated with a single element of the state-estimate $\hat{\boldsymbol{x}}_d$, *i.e.*, for the phase and Doppler of a single ray. Accordingly,

$$\mathrm{Var}(\hat{\nu}_{l,d}) > \left(J_d^{\nu\nu}\right)^{-1}, \quad (41)$$

$$\mathrm{Var}(\hat{\varphi}_{l,d}) > \left(J_d^{\varphi\varphi}\right)^{-1}. \quad (42)$$

In Fig. 3 and Fig. 4 we plot the BCRB and variance for the Doppler rate and phase terms, respectively. The variance of the observation noise is $\sigma_v^2 = 0.1$, a single path, *i.e.*, $L = 1$, initial phase $\varphi_{l,0} \sim U[-\pi, \pi]$, and the Doppler rate $\nu = 0.01$.

In Fig. 5 we plot the BCRB and the variance of the Doppler term estimate while considering different values for the Doppler term and the for the variance of the observation noise. Respectively, $\nu \in [0.01, 1]$ and $\sigma_v^2 = \{0.1, 0.15, 0.25\}$. By inspecting Fig. 5 we can see that there is a close agreement between the BCRB and EKF performance when the Doppler term is small (e.g., $\nu \in [0.01, 0.1]$), and the variance of the observation noise is also small (e.g., $\sigma_v^2 \leq 0.1$). However, when larger values of ν and σ_v^2 are considered this agreement is lost and the EKF performance degrades rapidly. Similar results were obtained for the estimate of the phase term.

IV. PERFORMANCE RESULTS

The parameters used on the simulations are listed in Table 3 and the vehicle velocities with the associated Doppler rates in Table 4, for perspective. The channel gains $\{\alpha_l;\ l = 0, 1, \ldots, L-1\}$ where generated according to the circularly symmetric Gaussian distribution $\mathcal{CN}(0, \sigma_\alpha^2)$, with $\sigma_\alpha^2 = 1$. No channel coding is used.

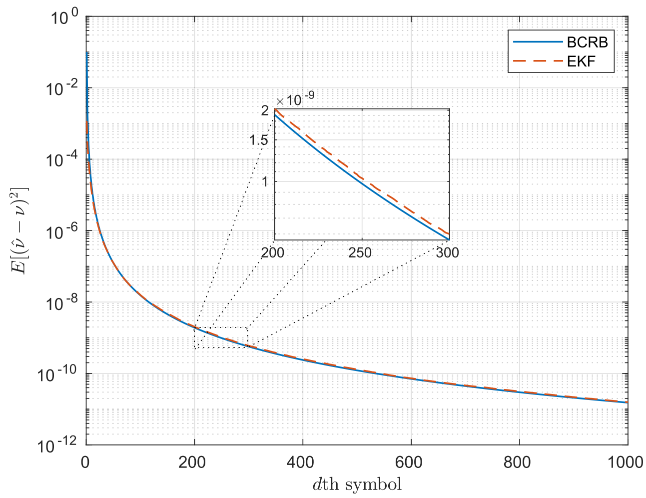

FIGURE 3. BCRB and variance of the estimate for the Doppler rate term with respect to the recursion number.

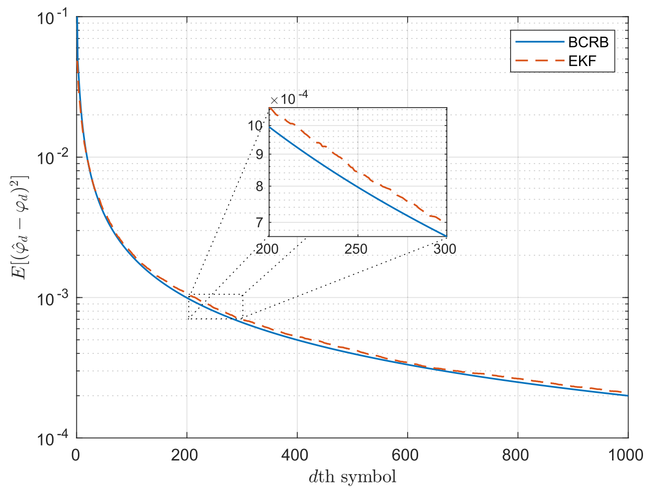

FIGURE 4. BCRB and variance of the estimate for the phase term with respect to the recursion number.

TABLE 3. Simulation parameters.

Parameter	Value
Modulation	QPSK
DFT-size	$N = 256$ modulation symbols
Frame size	$N_{\mathrm{sym}} = 300$ symbols
Number of rays	$L = 16$ rays
Size of training stage	$N_{\mathrm{train}} = 30$ symbols
Training symbol period	$p = 10$ symbols

TABLE 4. Velocity $\Delta v = \frac{\Delta f}{f_c} c$.

Doppler shift $\nu = \Delta f T_{\mathrm{B}}$	0.01	0.03	0.05	0.1
Velocity* [km/h]	25	76	126	252

$^*f_c = 6\,\mathrm{GHz};\ T_{\mathrm{B}} = 1/14\,\mathrm{ms}$

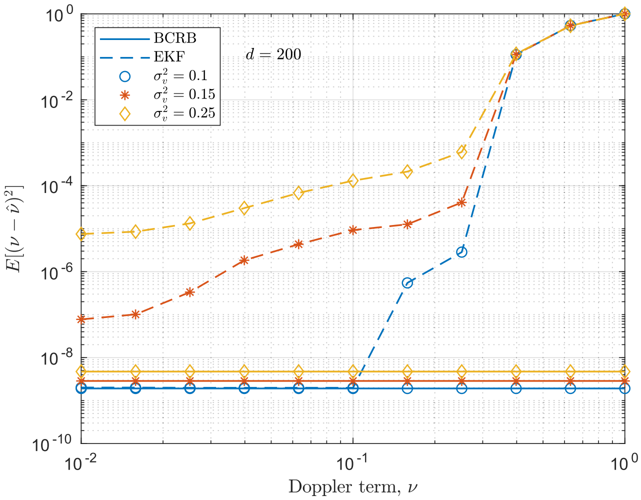

FIGURE 5. BCRB and variance of the estimate for the Doppler rate term for the recursion $d = 200$, observation noise variance $\sigma_v^2 = \{0.1, 0.15, 0.25\}$, and the Doppler term $\nu \in [0.01, 1]$.

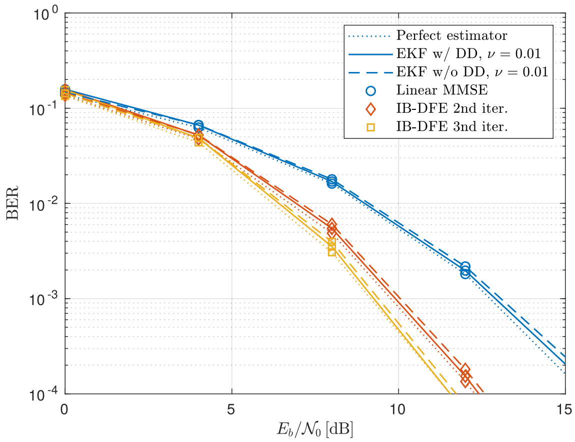

FIGURE 6. BER *vs.* the $E_b/\mathcal{N}_0$ for $\nu = 0.01$.

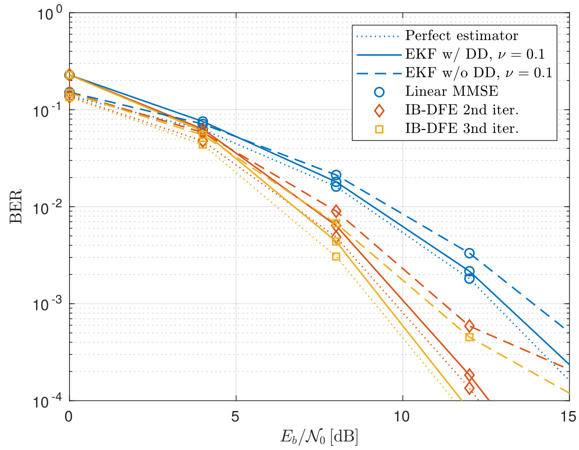

FIGURE 7. BER *vs.* the $E_b/\mathcal{N}_0$ for $\nu = 0.1$.

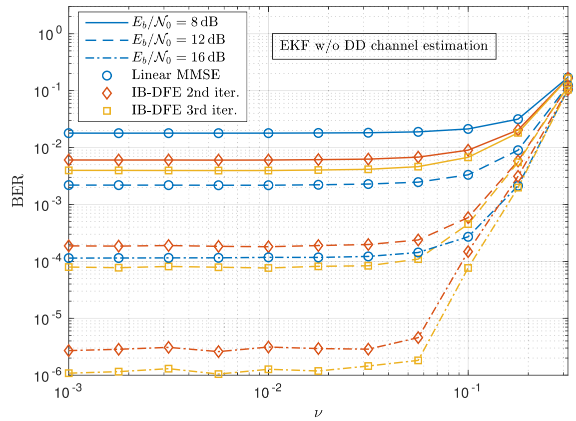

FIGURE 8. BER *vs.* the Doppler term ν for the EKF without DD channel estimation.

Fig. 6 depicts the BER curves corresponding to a normalized Doppler term $\nu = 0.01$ for three different situations. Firstly, we consider the SC-FDE transmission using a perfect channel estimator (*i.e.*, the filtering coefficients of the IB-DFE are derived using the true CFR). Secondly, we consider that the channel tracking is done using an EKF without DD channel estimation (EKF w/o DD). Thirdly and finally, we consider that the channel tracking is done using an EKF with DD channel estimation (EKF w/ DD). Additionally, we consider that the channel equalization is conducted through three iterations of the IB-DFE. By inspecting Fig. 6, we can see that there is a close agreement between the curves associated with the EKF and those associated with the perfect channel estimation, revealing that the EKF is capable of tracking effectively the variations of the channel when a small Doppler term (*e.g*, $\nu = 0.01$) is present.

Fig. 7 depicts the BER curves corresponding to a normalized Doppler term $\nu = 0.1$. This figure is similar to Fig. 6 with the only difference being the value of the normalized Doppler term, which is considerably larger now. By inspecting Fig. 7 we see that the EKF with DD channel estimation displays a BER close to the ideal case with almost no loss in performance. Regarding the EKF without DD channel estimation, a small performance degradation occurs.

Fig. 8 depicts the BER *vs.* the normalized Doppler term ν. This figure provides a graphical reference on the range of Doppler values supported by the system. Particularly, for the EKF without DD channel estimation. By inspecting Fig. 8 we can see that the BER performance remains practically unaltered for Doppler values up to $\nu = 0.06$. This Doppler value corresponds to a velocity of more than 120 km/h when considering a carrier frequency of $f_c = 6$ GHz and a block duration $T_B = 1/14$ ms. We will see next that with DD channel estimation this range can be increased.

Fig. 9 depicts the BER *vs.* the normalized Doppler term ν for the EKF with DD channel estimation. Once again, this figure provides a graphical reference on the range of Doppler values supported by the system. By inspecting Fig. 9, we can see that the BER performance remains practically unaltered for Doppler values up to $\nu = 0.1$. This is a very large Doppler. In fact if we look up Table 4 we see that this normalized

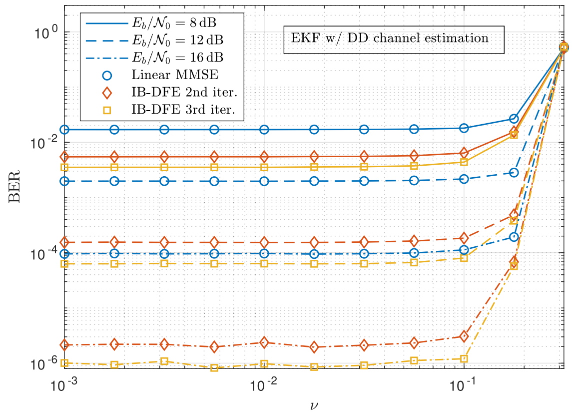

FIGURE 9. BER *vs.* the Doppler term ν for the EKF with DD channel estimation.

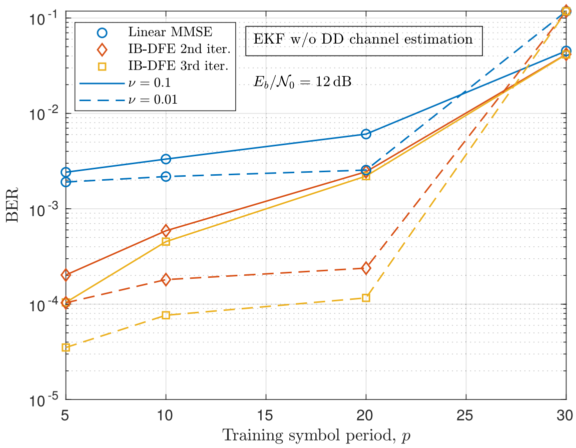

FIGURE 10. BER *vs.* the training symbol period p for the EKF without DD channel estimation.

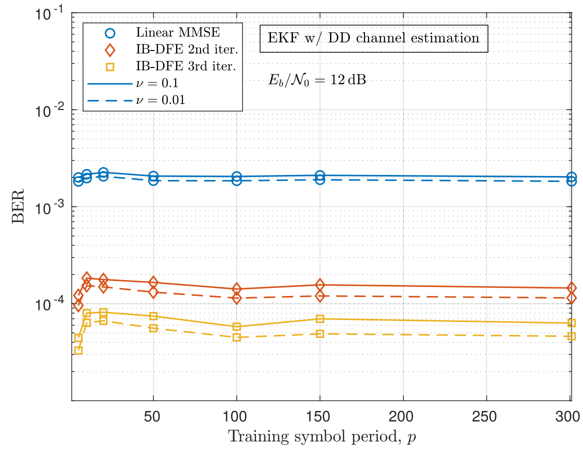

FIGURE 11. BER *vs.* the training symbol period p for the EKF with DD channel estimation.

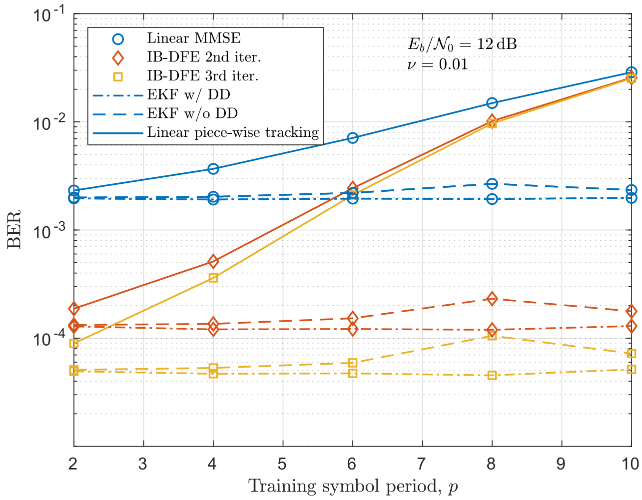

FIGURE 12. BER *vs.* the training symbol period, p, for the linear piece-wise channel tracking.

Doppler value corresponds to a velocity of approximately 250 km/h, when considering a carrier frequency of $f_c = 6\,\mathrm{GHz}$ and a block duration of $T_{\mathrm{B}} = 1/14\,\mathrm{ms}$. Clearly, a velocity only common in high-speed trains.

Fig. 10 depicts the evolution of the BER *vs.* the training symbol period, p, for the EKF without DD channel estimation. We see that if the normalized Doppler term is small enough (*e.g.*, $\nu = 0.01$) the BER does not vary significantly with the training symbol period. If, on the contrary, the Doppler term is large (*e.g.*, $\nu = 0.1$) then a training symbol period up to $p = 10$ is more appropriate since significant performance degradation may occur for larger values of p.

Similarly to Fig. 10, Fig. 11 depicts the evolution of the BER *vs.* the training symbol period, p, but this time for the EKF with DD channel estimation. Comparing both figures we see that the differences are significant. In fact, the EKF with DD channel estimation is practically unresponsive to changes in the training symbol period value. Note that, the last value of the training symbol period in the graph is $p = 301$ symbols, which is larger than the frame size considered, $N_{\mathrm{frame}} = 300$ symbols. Therefore, after the initial training stage, no other training symbol is transmitted and still the system displays no meaningful performance loss.

In Fig. 12 we plot the the BER performance *vs.* the training symbol period, p, when the channel estimates are obtained using the EKF with the decision-directed approach (EKF w/ DD), the EKF without the decision-directed approach (EKF w/o DD), and a linear piece-wise channel tracking solution. We use this last channel tracking solution to show the performance gain obtained through the use of the EKF.

By inspecting Fig. 12 we see that the linear piece-wise channel tracking is very sensitive to the presence of Doppler shifts. In fact, for a normalized Doppler $\nu = 0.01$, and $E_b/\mathcal{N}_0 = 12\,\mathrm{dB}$, we only have BER performances comparable to the ones obtained with the EKF when one in two symbols is a training symbol, i.e., $p = 2$, which is manifestly unaffordable in terms of overheads. These results clearly justify the need for appropriate channel tracking (e.g., through the use of the EKF) even when the Doppler shifts are small.

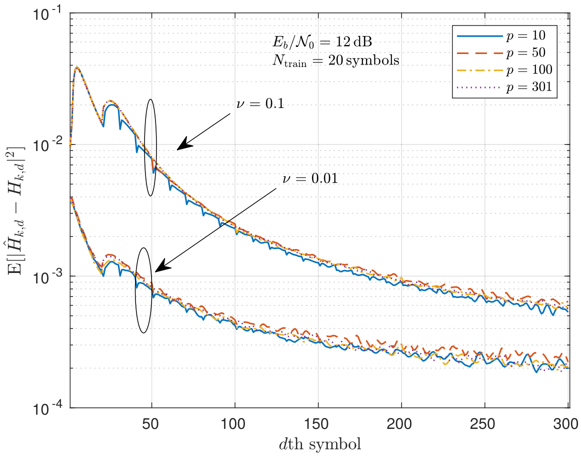

FIGURE 13. MSE for different training symbol period *p*.

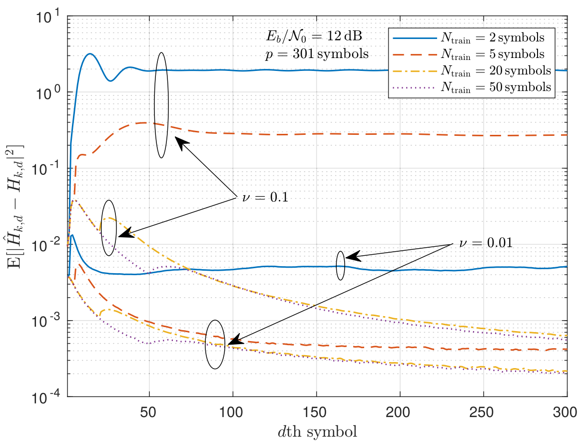

FIGURE 14. MSE for different sizes of the initial training stage, N_{train}.

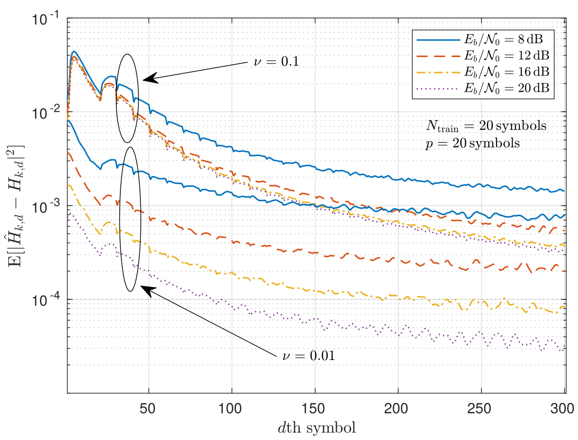

FIGURE 15. MSE for different values of $E_b/\mathcal{N}_0$.

Note that in Fig. 13, Fig. 14, and Fig. 15, we will be considering only the EKF with DD channel estimation case for brevity.

Fig. 13 traces the MSE of the CFR estimate $\mathrm{E}[|\hat{H}_{k,d} - H_{k,d}|^2]$ for different values of the training symbol period p and for $E_b/\mathcal{N}_0 = 12$ dB, $\nu = \{0.01, 0.1\}$, and an initial training stage of $N_{\text{train}} = 20$ symbols. By inspecting the figure, it is clear that the EKF with DD channel estimation is practically unresponsive to the presence of further training symbols after the initial training stage.

In Fig. 14, we plot the MSE considering different sizes for the initial training stage. Namely, $N_{\text{train}} = \{2, 5, 20, 50\}$. Exactly to evaluate the impact of the size of the initial training stage on the system performance. As expected, the larger the training stage the faster the filter convergence.

Finally, in Fig. 15 we plot the MSE for different values of $E_b/\mathcal{N}_0$, namely $E_b/\mathcal{N}_0 = \{8, 12, 16, 20\}$ dB and the normalized Doppler terms of $\nu = \{0.01, 0.1\}$. For a large Doppler (*e.g.*, $\nu = 0.1$), the impact on the MSE from varying the $E_b/\mathcal{N}_0$ is less evident than if the Doppler is small (*e.g.*, $\nu = 0.01$). In this latter case, the MSE is already small value and increasing the $E_b/\mathcal{N}_0$ will bring it further down.

V. CONCLUSION

With this work we proposed a channel equalization and tracking scheme, where the IB-DFE deals with the ISI and the EKF with the time-varying nature of the channel. We designed an efficient frame structure, suitable for V2X communications, and showed that it is possible to limit channel estimation overheads. We also showed that these overheads can be further reduced if a decision-directed approach is considered. In fact, we showed that using the decision-directed approach ensures that no further training symbols are required besides those used in the initial training stage.

ACKNOWLEDGMENT

This article was presented at the 2019 IEEE 90th Vehicular Technology Conference.

REFERENCES

[1] M. Boban, A. Kousaridas, K. Manolakis, J. Eichinger, and W. Xu, "Connected roads of the future: Use cases, requirements, and design considerations for vehicle-to-everything communications," *IEEE Veh. Technol. Mag.*, vol. 13, no. 3, pp. 110–123, Sep. 2018.

[2] P. K. Singh, S. K. Nandi, and S. Nandi, "A tutorial survey on vehicular communication state of the art, and future research directions," *Veh. Commun.*, vol. 18, Aug. 2019, Art. no. 100164.

[3] O. Kaiwartya, A. H. Abdullah, Y. Cao, A. Altameem, M. Prasad, C.-T. Lin, and X. Liu, "Internet of Vehicles: Motivation, layered architecture, network model, challenges, and future aspects," *IEEE Access*, vol. 4, pp. 5356–5373, 2016.

[4] T. Mekki, I. Jabri, A. Rachedi, and M. Ben Jemaa, "Vehicular cloud networks: Challenges, architectures, and future directions," *Veh. Commun.*, vol. 9, pp. 268–280, Jul. 2017.

[5] S. Monhof, M. Haferkamp, B. Sliwa, and C. Wietfeld, "Payload-size and deadline-aware scheduling for upcoming 5G networks: Experimental validation in high-load scenarios," in *Proc. IEEE 88th Veh. Technol. Conf. (VTC-Fall)*, Aug. 2018, pp. 1–5.

[6] P. Keshavamurthy, E. Pateromichelakis, D. Dahlhaus, and C. Zhou, "Cloud-enabled radio resource management for co-operative driving vehicular networks," in *Proc. IEEE Wireless Commun. Netw. Conf. (WCNC)*, Apr. 2019, pp. 1–6.

[7] P. Keshavamurthy, P. Spapis, D. Dahlhaus, and C. Zhou, "Session-enabled joint radio resource selection for co-operative automated driving," in *Proc. IEEE 89th Veh. Technol. Conf. (VTC-Spring)*, Apr. 2019, pp. 1–5.

[8] X. Wang, S. Mao, and M. X. Gong, "An overview of 3GPP cellular vehicle-to-everything standards," *GetMobile, Mobile Comput. Commun.*, vol. 21, no. 3, pp. 19–25, Nov. 2017.

[9] L. G. Baltar, M. Mueck, and D. Sabella, "Heterogeneous vehicular communications-multi-standard solutions to enable interoperability," in *Proc. IEEE Conf. Standards Commun. Netw. (CSCN)*, Oct. 2018, pp. 1–6.
[10] *Study on Enhancement of 3GPP Support for 5G V2X Services*, document TR 22.886, 3GPP, 2016.
[11] *Study on Enhancement of Ultra-Reliable Low-Latency Communication (URLLC) Support in the 5G Core Network (5GC)*, document TR 23.725, 3GPP, 2018.
[12] *Architecture Enhancements for 5G System (5GS) to Support Vehicle-to-Everything (V2X) Services*, document TS 23.287, 3GPP, 2018.
[13] *Study on Enhancements to Application Layer Support for V2X Services*, document TR 23.764, 3GPP, 2019.
[14] C. F. Mecklenbrauker, A. F. Molisch, J. Karedal, F. Tufvesson, A. Paier, L. Bernado, T. Zemen, O. Klemp, and N. Czink, "Vehicular channel characterization and its implications for wireless system design and performance," *Proc. IEEE*, vol. 99, no. 7, pp. 1189–1212, Jul. 2011.
[15] F. Jameel, S. Wyne, S. J. Nawaz, and Z. Chang, "Propagation channels for mmWave vehicular communications: State-of-the-art and future research directions," *IEEE Wireless Commun.*, vol. 26, no. 1, pp. 144–150, Feb. 2019.
[16] F. J. Martin-Vega, M. C. Aguayo-Torres, G. Gomez, J. T. Entrambasaguas, and T. Q. Duong, "Key technologies, modeling approaches, and challenges for millimeter-wave vehicular communications," *IEEE Commun. Mag.*, vol. 56, no. 10, pp. 28–35, Oct. 2018.
[17] H. Sari, G. Karam, and I. Jeanclaude, "An analysis of orthogonal frequency-division multiplexing for mobile radio applications," in *Proc. IEEE Veh. Technol. Conf. (VTC)*, Stockholm, Sweden, Jun. 1994, pp. 1635–1639.
[18] A. Gusmao, R. Dinis, J. Conceicao, and N. Esteves, "Comparison of two modulation choices for broadband wireless communications," in *Proc. IEEE 51st Veh. Technol. Conf. (VTC-Spring)*, Tokyo, Japan, vol. 2, May 2000, pp. 1300–1305.
[19] D. Falconer, S. L. Ariyavisitakul, A. Benyamin-Seeyar, and B. Eidson, "Frequency domain equalization for single-carrier broadband wireless systems," *IEEE Commun. Mag.*, vol. 40, no. 4, pp. 58–66, Apr. 2002.
[20] N. Benvenuto, R. Dinis, D. Falconer, and S. Tomasin, "Single carrier modulation with nonlinear frequency domain equalization: An idea whose time has come—Again," *Proc. IEEE*, vol. 98, no. 1, pp. 69–96, Jan. 2010.
[21] M. Tuchler, R. Koetter, and A. C. Singer, "Turbo equalization: Principles and new results," *IEEE Trans. Commun.*, vol. 50, no. 5, pp. 754–767, May 2002.
[22] R. A. Iltis, "Joint estimation of PN code delay and multipath using the extended Kalman filter," *IEEE Trans. Commun.*, vol. 38, no. 10, pp. 1677–1685, Oct. 1990.
[23] S. Haykin, A. H. Sayed, J. R. Zeidler, P. Yee, and P. C. Wei, "Adaptive tracking of linear time-variant systems by extended RLS algorithms," *IEEE Trans. Signal Process.*, vol. 45, no. 5, pp. 1118–1128, May 1997.
[24] C. Komninakis, C. Fragouli, A. H. Sayed, and R. D. Wesel, "Multi-input multi-output fading channel tracking and equalization using Kalman estimation," *IEEE Trans. Signal Process.*, vol. 50, no. 5, pp. 1065–1076, May 2002.
[25] E. P. Simon, L. Ros, H. Hijazi, J. Fang, D. P. Gaillot, and M. Berbineau, "Joint carrier frequency offset and fast time-varying channel estimation for MIMO-OFDM systems," *IEEE Trans. Veh. Technol.*, vol. 60, no. 3, pp. 955–965, Mar. 2011.
[26] E. P. Simon and M. A. Khalighi, "Iterative soft-Kalman channel estimation for fast time-varying MIMO-OFDM channels," *IEEE Wireless Commun. Lett.*, vol. 2, no. 6, pp. 599–602, Dec. 2013.
[27] Y. Liao, X. Shen, X. Dai, M. Zhao, K. Liu, D. Li, and X. Zhou, "EKF-based joint channel estimation and decoding design for non-stationary OFDM channel," in *Proc. IEEE Global Commun. Conf. (GLOBECOM)*, Singapore, Dec. 2017, pp. 1–6.
[28] H. Kim and J. Tugnait, "Turbo equalization for doubly-selective fading channels using nonlinear Kalman filtering and basis expansion models," *IEEE Trans. Wireless Commun.*, vol. 9, no. 6, pp. 2076–2087, Jun. 2010.
[29] Q. Shi, N. Wu, X. Ma, and H. Wang, "Frequency-domain joint channel estimation and decoding for faster-than-Nyquist signaling," *IEEE Trans. Commun.*, vol. 66, no. 2, pp. 781–795, Feb. 2018.
[30] P. Pedrosa, R. Dinis, D. Castanheira, A. Silva, and A. Gameiro, "Joint channel equalization and tracking for SC-FDE schemes," in *Proc. IEEE 90th Veh. Technol. Conf. (VTC-Fall)*, Sep. 2019, pp. 1–6.
[31] P. Pedrosa, R. Dinis, A. Rodrigues, and F. Nunes, "Joint frequency domain equalisation and phase noise estimation for single-carrier modulations in doubly-selective channels," *IET Commun.*, vol. 9, no. 8, pp. 1138–1146, May 2015.
[32] R. Dinis, A. Gusmo, and N. Esteves, "On broadband block transmission over strongly frequency-selective fading channels," in *Proc. Int. Conf. Wireless Commun.*, Calgary, AB, Canada, Jul. 2003, pp. 261–269.
[33] P. Montezuma, F. Silva, and R. Dinis, *Frequency-Domain Receiver Design for Doubly Selective Channels*. Boca Raton, FL, USA: CRC Press, 2019.
[34] F. Silva, R. Dinis, and P. Montezuma, "Estimation of the feedback reliability for IB-DFE receivers," *ISRN Commun. Netw.*, vol. 2011, Aug. 2011, Art. no. 980830
[35] S. M. Kay, *Fundamentals Stat. Signal Processing: Estimation Theory*. Upper Saddle River, NJ, USA: Prentice-Hall, 1993.
[36] P. Tichavsky, C. H. Muravchik, and A. Nehorai, "Posterior Cramer–Rao bounds for discrete-time nonlinear filtering," *IEEE Trans. Signal Process.*, vol. 46, no. 5, pp. 1386–1396, May 1998.

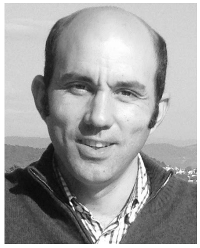

PEDRO PEDROSA (Member, IEEE) was born in Luanda, Angola, in 1977. He received the M.Sc. and Ph.D. degrees in electrical and computer engineering from the Instituto Superior Técnico, Universidade de Lisboa, Lisbon, Portugal, in 2007 and 2012, respectively.

From 2008 to 2014, he was a Research Fellow with the Instituto de Telecomunicações (IT), Lisbon. From winter 2009 to 2010, he was a Visiting Student with the OPERA Department, Université libre de Bruxelles (ULB). In year 2014, he was a Research Fellow with the Laboratório de Pesquisas em Processamento Digital de Sinais, Universidade Federal de Santa Catarina (UFSC), Brazil. From 2015 to 2016, he was a Visiting Professor with the Post-Graduation Program in electrical engineering of UFSC. Since 2018, he has been a Researcher with IT, Aveiro, Portugal. His research interests are within the broad fields of signal processing and digital communications.

DANIEL CASTANHEIRA received the Licenciatura (ISCED level 5) and Ph.D. degrees in electronics and telecommunications from the University of Aveiro, in 2007 and 2012, respectively. In 2011, he was with the Departamento de Eletrónica, Telecomunicações e Informática at University of Aveiro, as an Assistant Professor. He is currently an Auxiliary Researcher with the Instituto the Telecomunicações, Aveiro, Portugal. He has been involved in several national and European Projects, namely RETIOT, SWING2, PURE-5GNET, HETCOP, COPWIN, PHOTON, within the FCT Portuguese National Scientific Foundation, and CODIV, FUTON, and QOSMOS with the FP7 ICT. His research interests are in signal processing techniques for digital communications, with emphasis for physical layer issues including channel coding, precoding/equalization, and interference cancelation.

ADÃO SILVA received the M.Sc. and Ph.D. degrees in electronics and telecommunications from the Universidade de Aveiro, in 2002 and 2007, respectively. He is currently an Assistant Professor with the Department of Electronics, Telecommunications and Informatics, Universidade de Aveiro, and also a Senior Researcher with the Instituto de Telecomunicações. He has been participating in several national and European projects, namely the ASILUM, MATRICE, 4MORE within the ICT programme and the FUTON and CODIV projects with the FP7 ICT. He has led several research projects, in the broadband wireless communications area, at the national level. He acted as a member of the TPC of several international conferences. His interests include multiuser MIMO, multicarrier-based systems, cooperative networks, precoding, multiuser detection, massive MIMO, and millimeter wave communications.

RUI DINIS (Senior Member, IEEE) received the Ph.D. degree from the Instituto Superior Técnico (IST), Technical University of Lisbon, Portugal, in 2001, and the Habilitation degree in telecommunications from the Faculdade de Ciências e Tecnologia (FCT), Universidade Nova de Lisboa (UNL), in 2010.

He was a Researcher with the Centro de Análise e Processamento de Sinal (CAPS), IST, from 1992 to 2005. From 2001 to 2008, he was a Professor with IST. In 2003, he was an Invited Professor with Carleton University, Ottawa, Canada. He was a Researcher with the Instituto de Sistemas e Robótica (ISR), from 2005 to 2008. Since 2009, he has been a Researcher with the Instituto de Telecomunicações (IT). He is currently an Associate Professor with FCT, Universidade Nova de Lisboa (UNL). He has been actively involved in several national and international research projects in the broadband wireless communications area. His research interests include transmission, estimation, and detection techniques.

Prof. Dinis was/is an Editor of the IEEE Transactions on Wireless Communications, the IEEE Transactions on Communications, the IEEE Transactions on Vehicular Technology, the IEEE Open Journal on Communications, and *Physical Communication* (Elsevier). He was also a Guest Editor of *Physical Communication* (Elsevier) (Special Issue on Broadband Single-Carrier Transmission Techniques). He is a VTS Distinguished Lecturer.

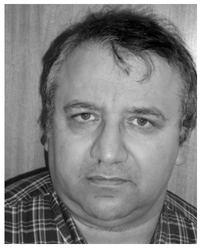

ATÍLIO GAMEIRO received the Licenciatura and Ph.D. degrees from the University of Aveiro, in 1985 and 1993, respectively. His industrial experience includes a period of one year with BT Labs and one year with NKT Elektronik. He is currently an Associate Professor with the Department of Electronics and Telecommunications, Universidade de Aveiro, and also a Researcher with the Instituto de Telecomunicações, Pólo de Aveiro, where he is also the Head of the group. He has published more than 200 technical articles in international journals and conferences. His current research activities involve space-time-frequency algorithms for the broadband wireless systems and cross-layer design. He has been involved and has led IT or the University of Aveiro participation on more than 20 national and European projects. His current research interests include signal processing techniques for digital communications and communication protocols, and within this research line he has done work for optical and mobile communications, either at the theoretical and experimental level.